Power Electronics and Drives
Volume 10(45), 2025 DOI: 10.2478/pead-2025-0022

Power Electronics and Drives

Data-Driven Optimisation Method for Tuning the HF Injection Parameters of an Extra Low Voltage Encoderless Synchronous Motor Drive

Research Paper

Hadj Ahmed Belghazali[1,2,*], Najla Haje Obeid[1], Eric Monmasson[2], Ngoc-Tu Trinh[1], Lahoucine Id-khajine[2]

[1]*IFP Energies nouvelles, Institut Carnot IFPEN Transports Energie, Electrical and Electronic Systems Department, Rueil-Malmaison, France*
[2]*SATIE Laboratory, CY Cergy Paris University, Cergy-Pontoise, France*

Received: 10 July, 2025; Received in the revised form: 05 September, 2025; Accepted: 17 September, 2025

Abstract: This paper discusses encoderless control of a permanent magnet synchronous machine that is fed by an extra-low DC bus voltage and operates within the low-speed range. The focus is on optimising the parameters of the high-frequency (HF) voltage injections necessary for estimating the electrical position of the rotor. Although the encoderless control method adopted is pulsating carrier voltage injection, the optimisation algorithm can be applied to other methods as well. The quality of the estimated position is influenced by the amplitude of the injected voltages, which also affect the disturbance of the machine torque. Therefore, this study aims to strike a balance between the quality of the estimated position and injection-related intrusion. The paper proposes an experimental approach to determining the optimal injection level, enabling accurate estimation of the electrical position while reducing torque disturbance. It also presents the experimental validation results of the optimal injection voltage implementation.

Keywords: *low speed encoderless control • extra low voltage machine • pulsating carrier signal injection • HF injection • voltage injection optimisation*

1. Introduction

In the context of prevailing environmental challenges, the electrification of systems has become imperative in various industrial sectors, particularly the automotive industry. The European Union has introduced legislation that enforces strict emission limits, thereby encouraging the adoption of electric vehicles. To satisfy these requirements, manufacturers are increasingly turning to permanent magnet motors, which have many advantages (Alfehaid et al., 2021; Lara et al., 2016). These motors are characterised by their high energy efficiency and power density. Their widespread use reflects an industrial approach that prioritises developing more sustainable solutions in line with objectives aimed at reducing carbon footprints.

These machines require precise knowledge of the rotor's position to function properly, which is usually obtained through the use of a position sensor. However, using such sensors has several disadvantages, including increased cost, reduced reliability and complex implementation. Encoderless control is a promising solution to these limitations. This approach can be divided into two main categories. The first category involves methods based on the machine model, which are effective in the medium and high-speed ranges. These methods rely on estimating the back electromotive force (back-EMF), either directly, where the back-EMF is used to obtain position information directly, as in Zhao et al. (2018), or indirectly, by relying on observers. For example, an enhanced perturbation observer was proposed by Song et al. (2016), and an extended Kalman filter was used by Pasqualotto et al. (2023).

* *Email: hadj-ahmed.belghazali@etu.cyu.fr*

The second category comprises methods based on magnetic salience, which are suitable for low speeds and standstill. These methods have been the subject of much research, both in terms of observer type, as in Corley and Lorenz (1998), where a Luenberger-type observer was implemented, and in terms of high-frequency (HF) injection type. The scientific literature contains many injection variants. For instance, in Mizutani et al. (1998), the rotor position and speed are estimated using an intermittent voltage pulse, whereas in Yoon et al. (2011), square-wave voltage injection is employed. In Tang et al. (2018), encoderless control is achieved by injecting bidirectional rotating HF carrier signals, while in Kim et al. (2016), the authors use a HF rotating voltage and propose a proper demodulation method to extract the rotor position from current signals. Carrier HF injection voltage can also be used, as in Liu and Zhu (2014), where the authors achieve injection in a stationary frame, whereas in Luo et al. (2016), the injection is realised in an estimated rotating frame. To improve this method, the Mai et al. (2021) use pulsating carrier injection and propose a position extraction strategy based on an amplitude observer. Furthermore, techniques have been developed that combine the previous two categories with artificial intelligence to enhance their effectiveness (Makni and Zine, 2016). These approaches offer flexibility by adapting to medium and high speeds, as well as low speeds and standstill (Zine et al., 2018b).

This article focuses on low speed, encoderless control methods that use HF voltage injections. Usually, the most convenient way to estimate speed is to measure the back-EMF of the motor since this quantity is proportional to the speed. However, at very low-speed the back-EMF is difficult to measure because it is very small. So other techniques like HF injection have to be used. Among the various injection techniques, the HF pulsating signal injection method has been adopted because of its numerous benefits (Raca et al., 2010), including its good performance and its simple position post-processing chain. This method relies on injecting a HF voltage and acquiring the stator's HF current in order to estimate the rotor's electric position. Therefore, estimation accuracy can be affected by the amplitude of the HF voltage signal (Khan and Mohammed, 2009). The study discussed in this article concerns an extra-low voltage machine for applications such as hybrid vehicles, license-free cars and soft mobility applications such as electric bicycles, which limits the maximum amplitude of the injection. High injection amplitudes introduce high harmonic currents and torque ripples. Based on the aforementioned references, the injection voltage amplitude is generally reported to be between 10 V and 20 V for low-voltage machines supplied with a DC bus voltage from 200 V to 400 V, equivalent to an interval of 2.5%–10% of the DC bus voltage. In extra low-voltage applications, the voltage injection must be reduced; however, the difficulty lies in choosing the correct injection amplitude. A very low amplitude may be affected by voltage drops in the inverter, while a high amplitude may disturb the machine torque. In our study, we investigated the impact of voltage injection amplitude by carrying out injections with an amplitude ranging from 1% to 8% of the DC bus voltage, equivalent to 0.5 V and 4 V.

The current study aims to improve position estimation and find the optimal injection amplitude for each operating point. Bibliographic research into enhancing the performance of encoderless control methods primarily focuses on injection or demodulation techniques. In Li et al. (2021), a HF signal injection scheme using an iterative learning algorithm was proposed to reduce HF torque ripples. Another way to improve the estimation performance is to optimise the injection parameters. In Petro et al. (2022), the authors propose a method of optimisation based on the root-mean-square error of the estimated position, speed and torque values achieved for a machine operating at a DC voltage of 325 V; however, it should be noted that these results were obtained via a MATLAB/Simulink (Mathworks) simulation and have not been validated experimentally. Another study, presented by Zine et al. (2018a), uses genetic algorithms to solve a parametric optimisation problem for an encoderless control method based on HF signal injection in an automotive application involving a 400 V machine.

This article proposes a data-driven optimisation method for calculating the amplitude of the injection voltage. The aim is to find the optimal balance between estimated rotor position quality and system disturbance for a given operating point. The proposed method relies on a reduced database supplemented by interpolations. Although it focuses on the pulsating carrier method, its principle can be extended to other types of HF voltage injection methods. The optimisation procedure presented below considers the mean position error, the variance of the estimated position error, the torque disturbance and the additional power losses consumed by the HF voltage injections. The article is organised as follows. First, the system under study is presented in Section 2. Section 3 provides a brief introduction to the pulsating carrier method. Section 4 details the HF voltage injection optimisation procedure. Finally, Section 5 presents the validation of the process and the experimental results of the tuned injection voltage implementation. Section 6 concludes the article and proposes future research.

2. Studied System

The test machine used in this study is a permanent magnet assisted synchronous reluctance (PMSynRel) machine with low salience. It is an extra-low-voltage machine that operates a DC bus voltage equal to 48 V. As shown in Figure 1, the test bench consists of two identical test machines mounted on the same shaft. The input DC supply voltage is 48 V, and the switching frequency of the voltage inverter is 12 kHz. To evaluate the position estimation performance, an inductive position sensor has been installed on each of the two machines. The characteristics of the test machine are given in Table 1.

3. Pulsating Carrier Signal Injection

Encoderless control, which utilises pulsating HF signal injections, is widely used in scientific literature for estimating rotor position (Cupertino et al., 2011). This technique involves superimposing a HF voltage, $V_h \cos(\omega_h t)$, onto the d-axis reference voltage, where V_h is the amplitude of the injected voltage and ω_h is its frequency. This additional voltage generates a HF current whose variations contain valuable information about the rotor position. To extract this information and guarantee machine controllability, the stator current is measured and analysed using adapted signal processing chains.

The first chain applies a series of filters and transformations to isolate the fundamental current, which is used for torque and current regulation. This approach ensures accurate machine control with minimal interference from the HF signals. Conversely, the second chain is dedicated to extracting the rotor's electrical position using information related to its error. In practice, the position error is sent to a phase-locked loop (PLL) to cancel it out, thereby estimating the rotor position and speed. Figure 2 summarises the operating principles of this position estimation method and the current regulation loop, while Figure 3 focuses on the PLL position and speed observer.

4. Voltage Injection Optimisation

4.1. Optimisation method

Belghazali et al. (2024) evaluates the various parameters influencing the performance of the pulsating carrier injection method. This study classifies these parameters into two main categories. The first category comprises

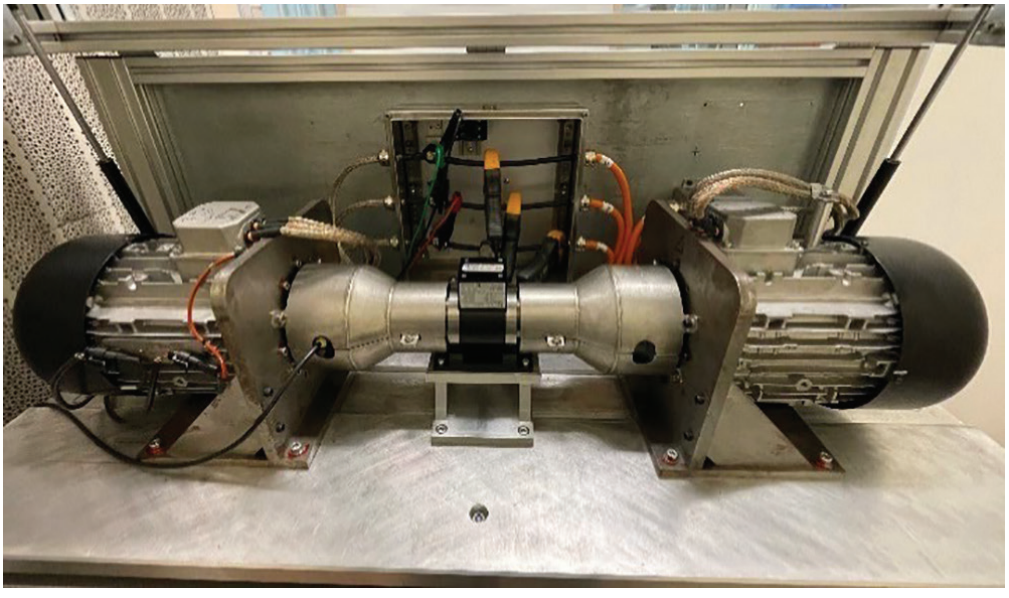

Figure 1. Experimental test bench.

Table 1. PMSynRel characteristics

Parameters	Values
Maximum speed	8,000 rpm
Maximum torque	10 N.m
Maximum current	120 A
Stator phase resistance	0.0021 Ω
Permanent magnet flux	5.3 mWb
Pole pairs number	8
L_d	18 µH
L_q	25 µH
L_{dq}(neglected since $\ll L_d$ and L_q)	0.08 µH

PMSynRel, permanent magnet assisted synchronous reluctance.

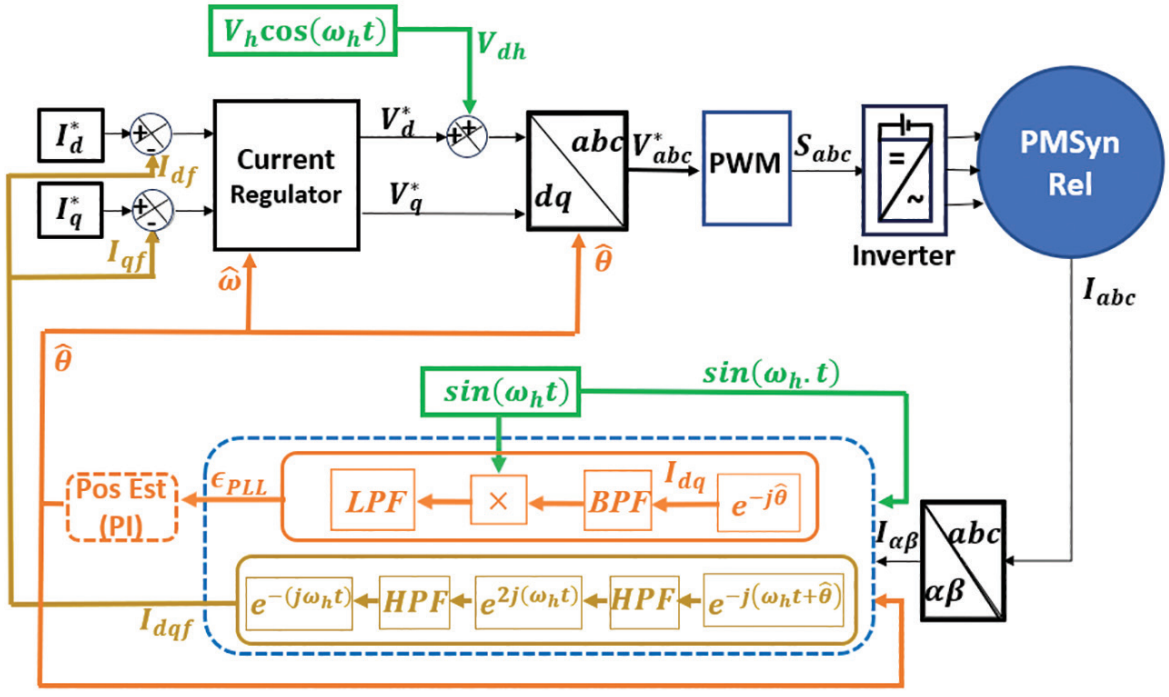

Figure 2. Global diagram of the position estimation and current control loops. PLL, phase-locked loop.(BPF: band-pass filter, HPF: high-pass filter, LPF: low-pass filter, PI: proportional and integral controller, PWM: pulse width modulation).

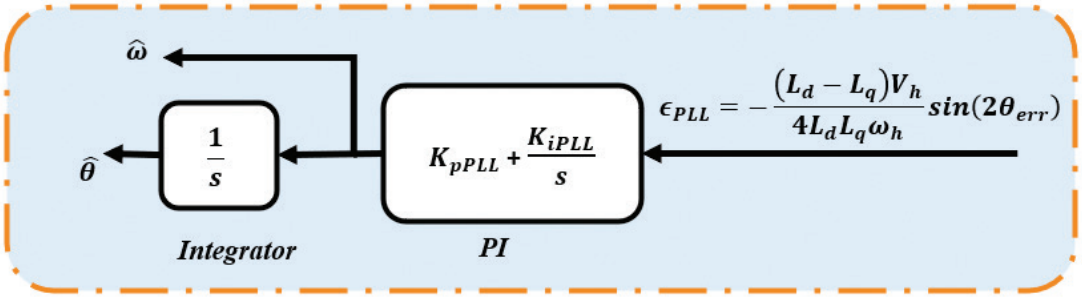

Figure 3. PLL position and speed observer. PLL, phase-locked loop.

parameters associated with HF injection conditions, such as the magnitude of the HF voltage and the frequency of the injected signal. The second category consists of parameters related to machine saliency. For the machine under study, the analysis showed that its saliency varied little with the applied load and thus had a limited impact on the performance of the position estimation method. The analysis also showed that a high injection frequency equal to 10% of the switching frequency of the voltage inverter significantly improves estimation performance compared to lower frequency values Belghazali et al. (2024) and that position error depends on the level of the injected voltage. For this reason, the injected frequency in this study is constant and set to the maximum possible with a switching frequency of 12 kHz. Taking these previous findings into account, this paper focuses solely on the influence of the injection amplitude, seeking to establish an optimal compromise between the level of intrusion due to the HF voltage injection and the quality of the position estimation.

Before presenting the optimisation algorithm, we will outline its specifications. The aim is to find the optimal compromise between 'Quality', which refers to the quality of the position estimation, and 'Cost', which refers to the cost of intrusion due to the injection process. Optimisation is performed over the operating range of (100 rpm → 500 rpm), which is equivalent to (1% → 6%) of the maximum speed of the machine, and for current amplitudes ranging from 0 A to 100 A (84% of the maximum current) in motor mode, and from 0 A to 50 A (42% of the maximum current) in generator mode. To differentiate between these two modes, the operating range is defined as (−50 A → 100 A). The optimisation process uses an experimental database acquired on the test bench. Data were gathered through multiple repetitive tests to ensure repeatability and enhance reliability. The collected data include estimated and measured positions, as well as measured torque and DC power. These were obtained for several V_h values ranging from 0.5 V to 4 V, equivalent to 1%–8% of the DC bus voltage and an injection frequency of 1,250 Hz. For the position estimation, the band-pass filter of Figure 2 was tuned with an adaptive cutting frequency equal to f_h, while the low-pass filter had a fixed cutting frequency equal to 150 Hz. For the current regulation loop, the cutting frequency of the two high-pass filters was set to 5 Hz. Figure 4 shows a summary of the tests used to create the database.

As mentioned above, the main objective is to strike the optimal balance between 'quality' and 'cost'. 'Quality' is defined by quantities that reflect the quality of position estimation. For a given operating point, these include the mean value of the position estimation error and the dispersion of the electrical position instantaneous value in relation to its mean. The expressions for 'quality' and 'cost' will be presented later in the article.

'Cost' represents the undesirable effects of voltage injection. For this category, power losses and torque disturbances generated by HF injections are considered. These factors are essential for assessing the impact of injection on the system's overall performance.

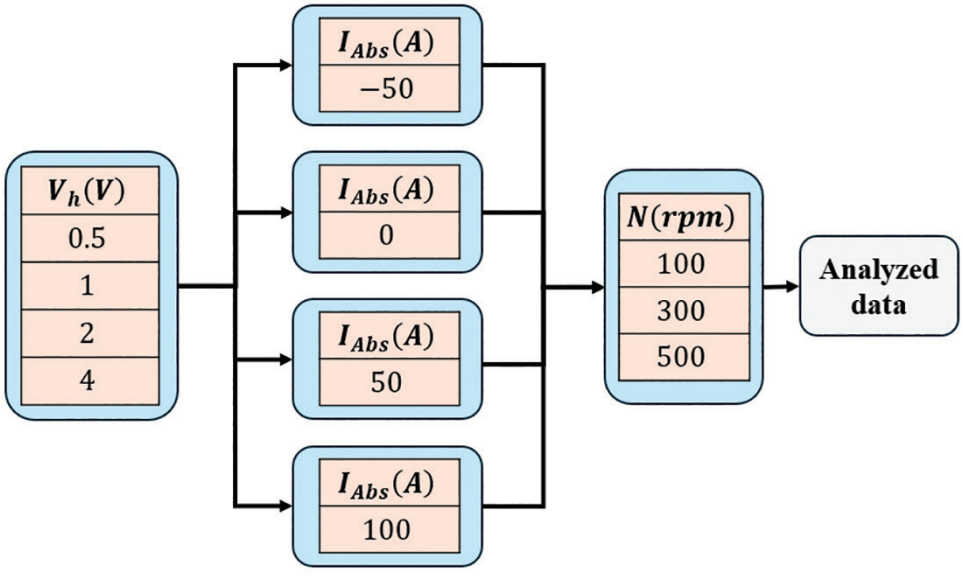

Figure 4. Experimental protocol for database acquisition.

To calculate the optimal injection voltage magnitude, the proposed *optimisation* method uses the quality quantities q_i and the cost quantities c_i as inputs. These quantities are then scaled to 'per unit' before being transformed into the final functions Q_{totPU} and C_{totPU}. Eqs (1) and (2) *summarise* this procedure, where w_{qi} and w_{cj} are the weights linked to quality and cost constraints, respectively. A study on the weighting of these terms will be presented later in this article, Section 4.2.

$$\begin{cases} q_{iPU} = \dfrac{q_i}{\mathrm{Max}\left(q_i\right)}, i = 1,2 \\ c_{jPU} = \dfrac{c_j}{\mathrm{Max}\left(c_j\right)}, j = 1,2 \end{cases} \tag{1}$$

$$\begin{cases} Q_{totPU} = \dfrac{\sum_i w_{qi}\ q_{iPU}}{\sum_i w_{qi}}, i = 1,2 \\ C_{totPU} = \dfrac{\sum_j w_{cj}\ C_{jPU}}{\sum_j w_{cj}}, j = 1,2 \end{cases} \tag{2}$$

Following numerical interpolation, the optimal injection voltage, noted V_{hOpti}, that reflects the best compromise between 'quality' and 'cost' is the one for which the quality and cost quantities are equivalent (Eq. 3). It was calculated using numerical interpolation to enrich the initial limited experimental database, built with a current step of 1 A and a V_h voltage step of 0.1 V (which is the injection accuracy limit).

$$Q_{totPU}\left(V_{hOpti}\right) - C_{totPU}\left(V_{hOpti}\right) = 0 \rightarrow V_{hOpti} \tag{3}$$

As the current dynamics are much higher than the speed dynamics, V_{hOpti} calculation is performed at a constant speed and expressed as a function of the stator current. A summary of the optimisation method is shown in Figure 5.

The data-driven optimisation method and the results obtained on the test bench are presented below. Several optimisation scenarios are presented to demonstrate the importance of each studied quantity and explain why certain variables are prioritised. The optimisation data were collected using experimental tests. The qualities and costs are studied as a function of the injection voltage, V_h, and the maximum current per stator phase, I_{Abs} (negative values

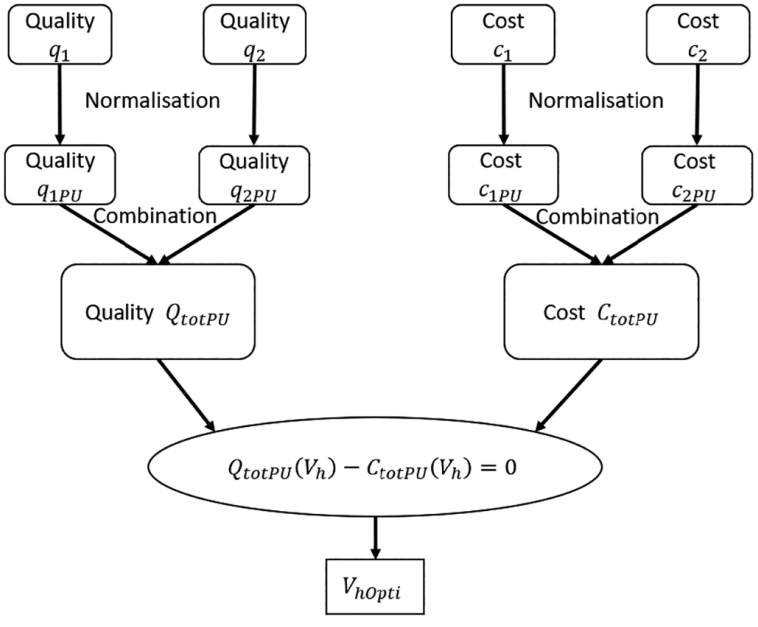

Figure 5. HF injection voltage optimisation flowchart. HF, high-frequency.

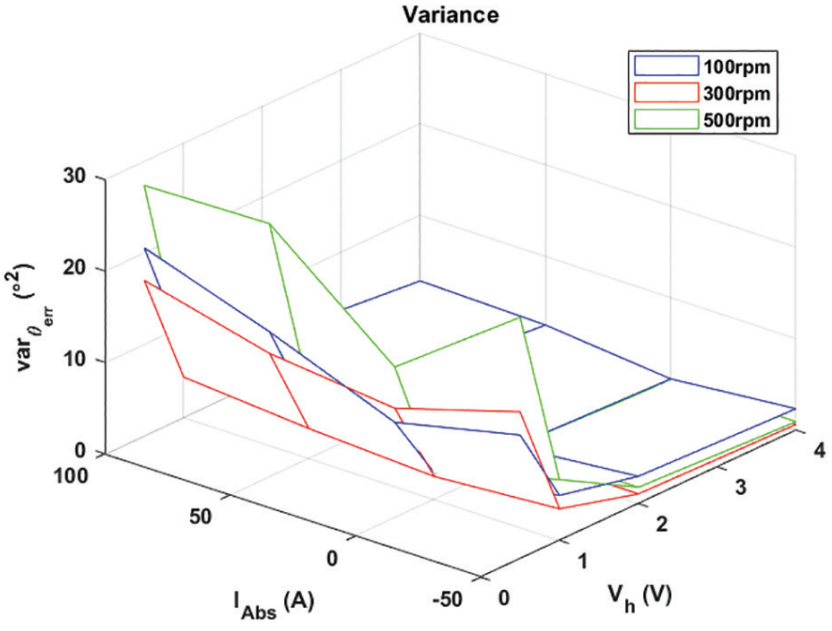

Figure 6. Variation of the variance of the estimated position error as a function of V_h and I_{Abs}.

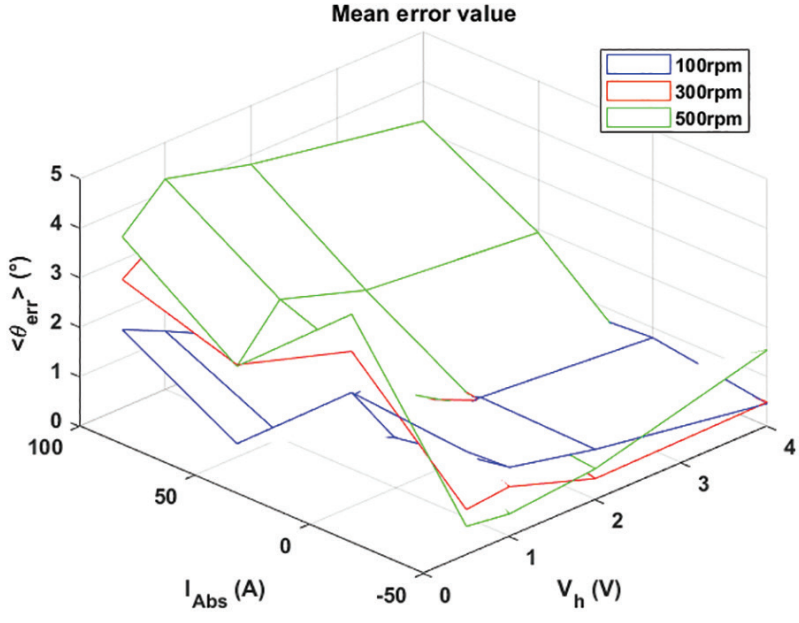

Figure 7. Variation of the mean error value as a function of V_h and I_{Abs}.

correspond to generator mode and positive values to motor mode), for three levels of mechanical speed. In the present study, two quality parameters were examined. The first, q_1, shown in Figure 6, is the variance of the estimated position error, which is related to positional dispersion. The second quantity, q_2, shown in Figure 7, is the average error between the measured and estimated positions. Furthermore, two quantities associated with the cost and intrusion of the injection method are also studied. The first, noted c_1 and presented in Figure 8, is the torque HF distortion rate. The second, noted as c_2 and shown in Figure 9, are the additional DC losses generated by the injection process.

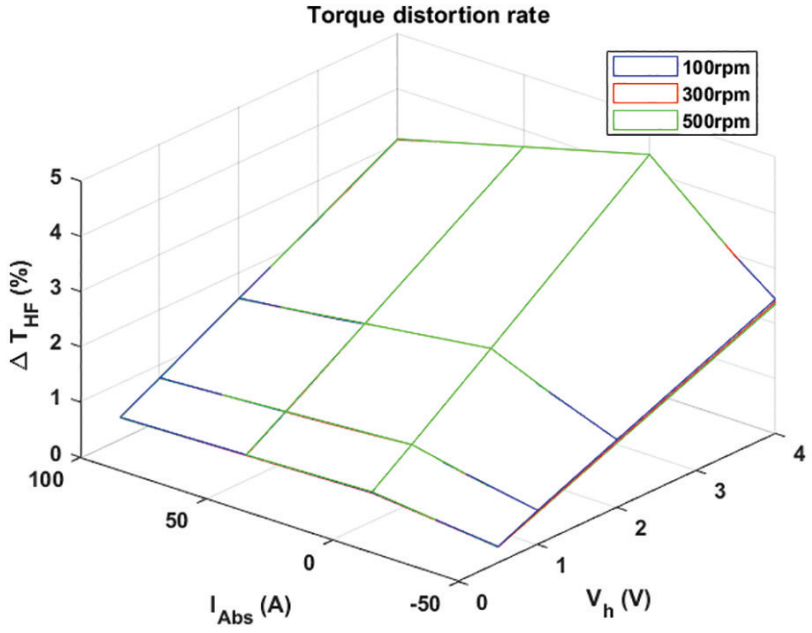

Figure 8. Variation of the torque distortion rate as a function of V_h and I_{Abs}.

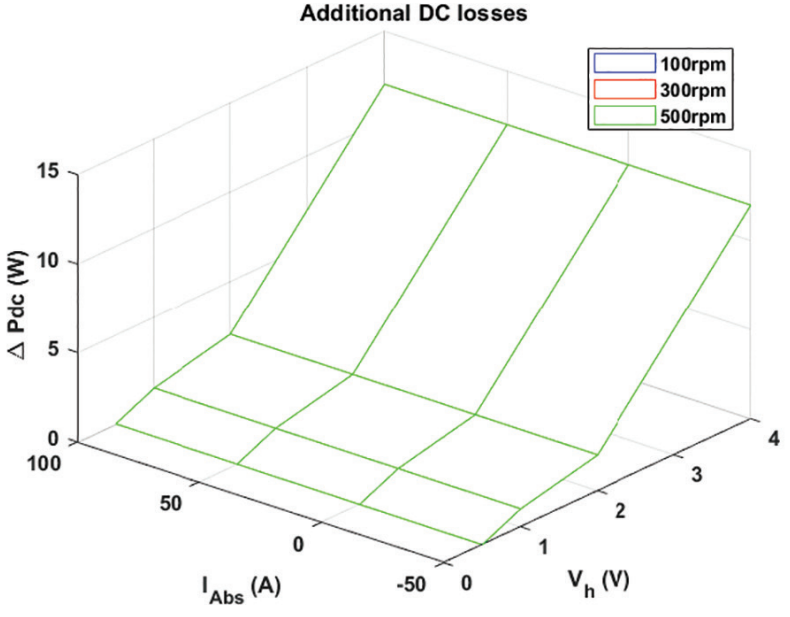

Figure 9. Variation of the additional DC losses as a function of V_h and I_{Abs}.

The position error, noted θ_{err}, between the estimated position, $\hat{\theta}$, and the position measured by the sensor, noted θ, is given by Eq. (4).

$$\theta_{err} = \hat{\theta} - \theta \tag{4}$$

Eqs (5) and (6) represent the mean and variance of the estimated position error, respectively, and are noted as θ_{err} and $var_{\theta_{err}}$. These are key indicators for assessing the accuracy of position estimation. These two variables

are calculated based on a time interval of 1.4 s, which is equivalent to an integer number of electrical periods and sampling points.

$$\langle \theta_{err} \rangle = \frac{1}{n} \sum_{k=1}^{n} \left(\theta_k - \hat{\theta}_k \right) \tag{5}$$

$$var_{\theta_{err}} = \frac{1}{n} \sum_{k=1}^{n} \left(\theta_{err\,k} - \theta_{err\,k} \right)^2 \tag{6}$$

The torque distortion calculation is based on both experimental data and analytical equations. This approach was chosen because the bandwidth of the torque meter does not permit reliable harmonic calculation. The expression for the electromagnetic torque, noted T_{em}, is presented in Eq. (7). At very low speeds, mechanical losses are considered negligible and the mechanical load torque is assumed to equal T_{em}.

$$T_{em} = \frac{3}{2} p \; i_q \left[\left(L_d \_ L_q \right) i_d + \psi_m \right] \tag{7}$$

The number of pole pairs in the test machine is p, the direct-axis inductance is L_d and the quadrature inductance is L_q, and the magnet equivalent flux is ψ_m.

In the presence of HF injections, the stator currents (i_d and i_q) can be expressed, in the real dq reference frame, as a function of the continuous components (i_{d0} and i_{q0}) and the injection-related components (i_{dh} and i_{qh}). The latter depend on the amplitude of V_h, the injection pulsation ω_h, and the error of the estimated position θ_{err}. The adopted model is a simplified version that does not include the cross-coupling inductance because it has been considered negligible compared to L_d and L_q. More detailed models are available that explicitly account for this cross-coupling inductance (Yousefi-Talouki et al., 2018). However, in our study this level of complexity was not required, since experimental measurements confirmed that L_{dq} remains negligible for the considered machine (see Table 1).

$$i_d = i_{d0} + i_{dh} \tag{8}$$

$$i_q = i_{q0} + i_{qh} \tag{9}$$

$$i_{dh} = \frac{1}{L_d} \frac{V_h}{\omega_h} \sin\left(\omega_h t \right) \cos\left(\theta_{err} \right) \tag{10}$$

$$i_{qh} = \frac{1}{L_q} \frac{V_h}{\omega_h} \sin\left(\omega_h t \right) \sin\left(\theta_{err} \right) \tag{11}$$

When $\theta_{err} \to 0$

$$i_d = i_{d0} + \frac{1}{L_d} \frac{V_h}{\omega_h} \sin\left(\omega_h t \right) \tag{12}$$

$$i_q = i_{q0} \tag{13}$$

Thus, the percentage disturbance due to the injection of V_h can be expressed as shown in Eqs (14) and (15). The results presented in this study were obtained by calculating the perturbation in the torque, ΔT_{HF}, as a function of the measured currents i_{dh}, i_{q0} and the measured mechanical torque. It should be noted that a more detailed formulation, which includes the cross-coupling inductance, has been proposed in Holczer et al. (2025). However, this additional level of detail was not required in our case for the same reason as the one exposed for the HF currents.

$$\Delta T_{HF} = \frac{\left(\frac{3}{2} P \; i_{q0} \left(L_d - L_q \right) i_{\mathrm{dh}} \right)}{T_{em}} \tag{14}$$

$$\Delta T_{HF}\left(\% \right) = 100 \left(\Delta T_{HF} \right) \tag{15}$$

Finally, the additional DC consumption, noted as ΔP_{dc}, is calculated using the DC power measured on the test bench in the presence of V_h injection (noted as P_{dcInj}) and the reference DC power for operation with a position sensor and without injection (noted as P_{dcRef}).

$$\Delta P_{dc} = P_{dcInj} - \mathrm{P_{dcRef}} \tag{16}$$

Using the data in Figures 6–9, along with a set of w_{qi} and w_{cj}, it is possible to calculate the total quality (Q_{totPU}) and the total cost (C_{totPU}), and thus the intersection between them (V_{hOpti}), for a given speed. This calculation is carried out for all the tested speeds (100, 300 and 500 rpm). Figure 10 shows an example of V_{hOpti} determination at 100 rpm: it corresponds to the intersection between the blue and pink curves when the quality factor level is equivalent to the cost level. However, this depends on how these factors are weighted. The selection of w_{qi} and w_{cj} is detailed in the next section.

4.2. Optimisation scenarios and results

In this section, we present the influence of the weights w_{qi} and w_{cj} on the calculation of V_{hOpti}. To emphasise the impact of the quality and cost variables under study, we present a step-by-step optimisation approach. All the results shown in this section were obtained with a numerical interpolation with a current step of 1 A, a V_h voltage step of 0.1 V and a speed step of 10 rpm. In the first scenario, denoted S1, the optimisation problem focuses on balancing the variance of the estimated position error (q_1) and the torque perturbation (c_1). In S1, $w_{q1} = w_{c1} = 1 \text{and} \, w_{q2} = w_{c2} = 0$. Figure 11 shows the results of calculating V_{hOpti} as a function of the machine speed and phase current. As the variance of the estimated position error depends slightly on the speed, and $\Delta T_{HF}(\%)$ is independent of it, the optimisation result is almost independent of speed; therefore, V_{hOpti} in S1 depends only on the stator phase current.

To visualise the impact of position error on V_h optimisation, scenario S2 considers the average position error, which is a speed-dependent parameter. Figure 12 shows the optimal injection voltage obtained with $w_{q1} = w_{q2} = w_{c1} = 1 \text{and} \, w_{c2} = 0$. The results show a slight increase in V_{hOpti} voltage values compared to S1 for speeds in the range between 300 rpm and 500 rpm, particularly when the current is high. This is understandable, as obtaining a better quality position estimation requires a higher injection voltage. Assigning greater weight to position accuracy and introducing the average position error accordingly increases the injection voltage.

Finally, in scenario S3, the DC losses generated by the injection are also considered with $w_{q1} = w_{q2} = w_{c1} = w_{c2} = 1$. As the voltage injections are relatively small, the DC losses generated are also relatively low. Figure 13 shows that considering the $\Delta \mathrm{P_{dc}}$ losses slightly modifies the optimisation results compared to scenario S2.

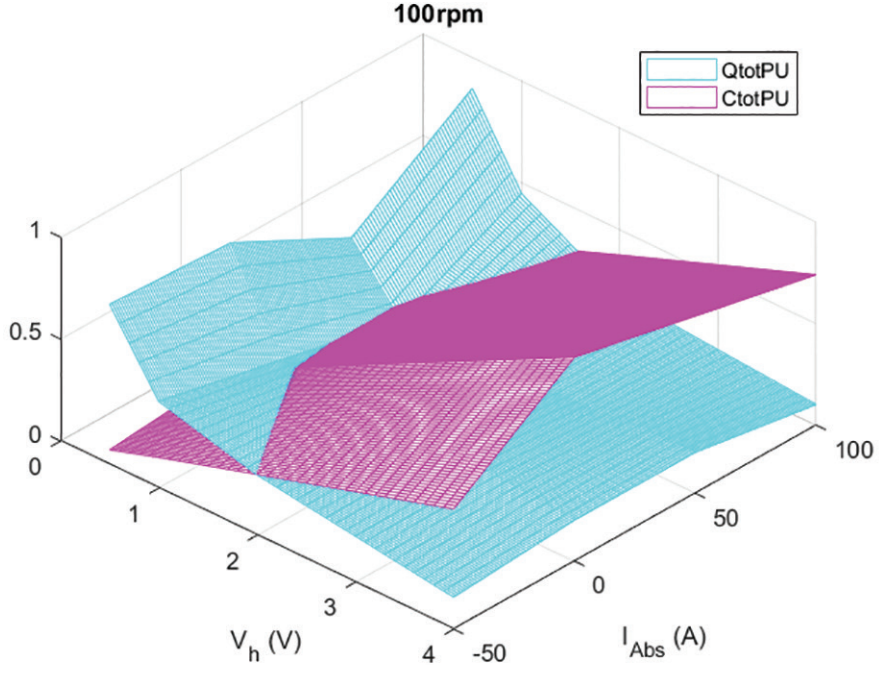

Figure 10. Example of V_{hOpti} calculation at 100 rpm.

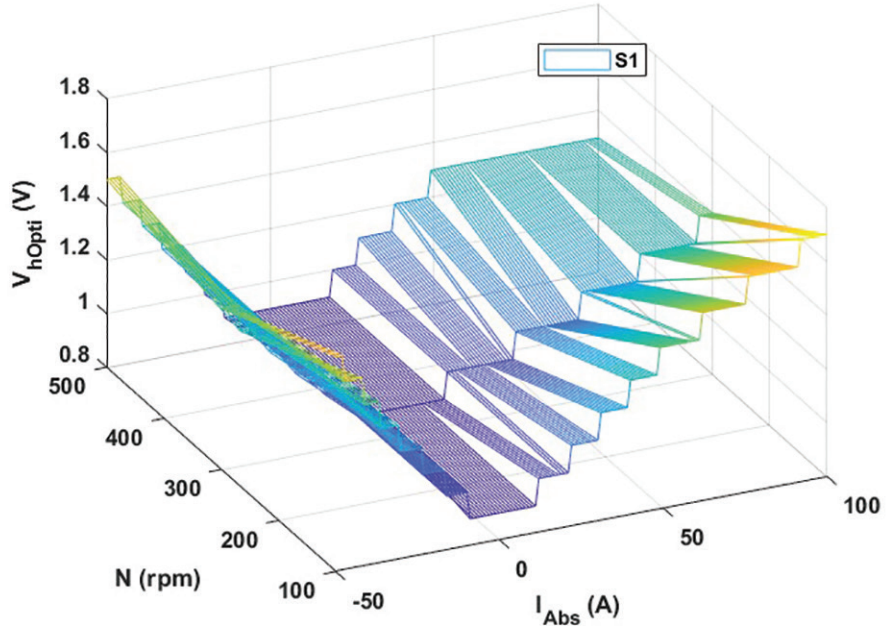

Figure 11. V_{hOpti} calculated with S1 scenario ($w_{q1} = w_{c1} = 1$ and $w_{q2} = w_{c2} = 0$).

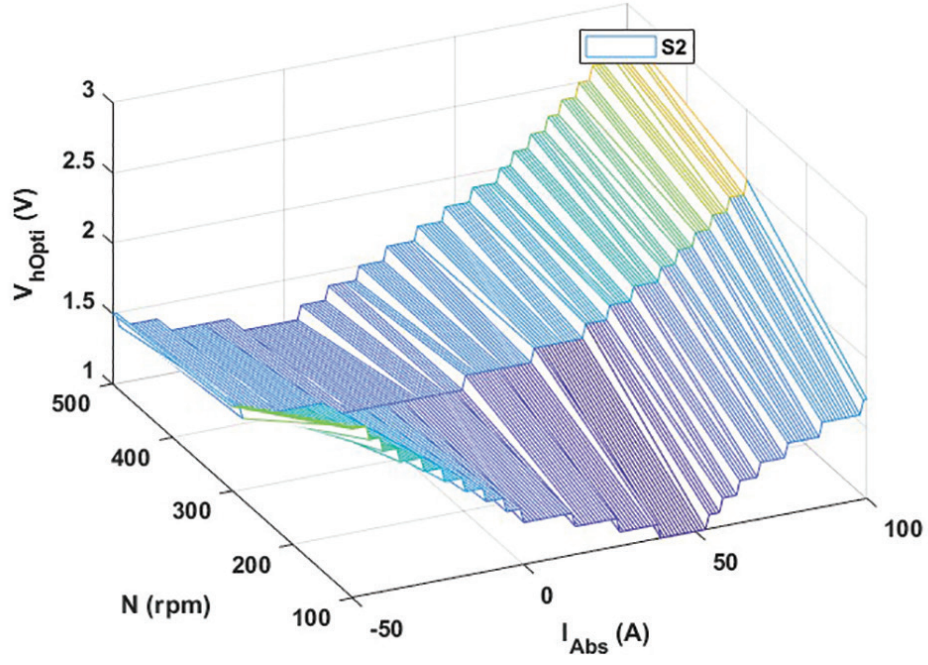

Figure 12. V_{hOpti} calculated with S2 scenario ($w_{q1} = w_{c1} = w_{q2} = 1$ and $= w_{c2} = 0$).

It should be noted that, for this study, all parameters were considered to have equal weighting in determining the optimal HF injection voltage. However, the impact of some parameters may be considered more significant than that of others. Figure 13 shows an example of the variation in the weights of ΔP_{dc} and ΔT_{HF}, obtained using the fourth optimisation scenario, S4, with $w_{q1} = w_{q2} = 1$, $w_{c1} = 2$ and $w_{c2} = 1$. Figure 13 presents a comparison of V_{hOpti} obtained with Scenarios S2, S3 and S4. These three scenarios produced similar results, with an increase in V_{hOpti} for S3 and S4 compared to S2.

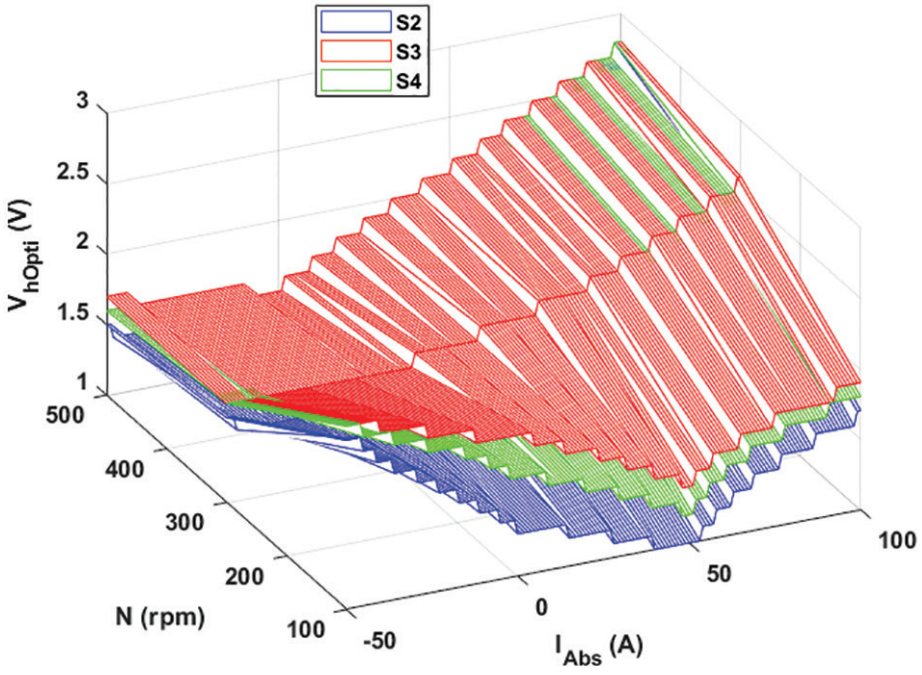

Figure 13. HF injection voltage amplitude for different scenarios. HF, high-frequency.

4.3. Experimental implementation of the optimisation

This section aims to validate the chosen V_{hOpti} strategy experimentally. The results obtained from scenario S2 have been adopted. As such, torque quality was prioritised over DC losses in terms of cost. Figure 14 presents the block diagram of the experimental implementation of V_{hOpti} using a look-up table (LUT).

Figures 15 and 16 show examples of the experimental implementation of V_{hOpti}. The slopes have been chosen in order to reproduce a standard dynamic behaviour of light electrical vehicle. Figure 15 shows an example of load variation ranging from −75 A to 120 A at a speed of 100 rpm with a current ramp of 200 A/s. It shows a comparison between the estimated and measured speed, the current load level in the (dq) reference frame, the variation of V_{hOpti} as a function of the operating point, and the position error. At 100 rpm, V_{hOpti} varies from 1 V to 2.2 V while maintaining correct speed estimation and a position error of <2°. Therefore, using a variable voltage injection does not affect speed or position estimation. In this figure, we can also observe that the position estimation error varies with the load but remains very low. This error depends on the amplitude of the HF injection as well as the modelling assumptions. The amplitude of the HF injection has been optimised to strike a balance between quality and cost. The modelling assumptions mainly concern the non-consideration of coupled cross-inductance, which is very small but not equal to zero. A similar observation can be made for Figure 16, which corresponds to a speed variation from 0 rpm to 500 rpm at a constant current load of 100 A with a speed ramp of 1000 rpm/s. As can be seen, the position estimation is operational at 0 rpm, which is outside the optimisation zone, with a position error of around 1°. At 100 A, V_{hOpti} increases with speed, varying from 1.8 V to 2.9 V, and offering a position error between 0° and 5°. As expected, Figure 16 also shows a direct correlation between the position estimation error and speed; the error increases with speed because the assumption of negligible back-EMF is no longer valid.

This optimum strategy is now being compared with the standard approach of using a constant amplitude injection voltage. This comparison is based on three criteria that determine the optimal injection voltage: the mean position error, the variance of the estimated position error, and the torque distortion rate. The comparison includes four V_h values: 0.5 V, 1 V, 2 V and 4 V.

It begins with an example at 100 rpm, with a current load varying from −50 A to 100 A. Figure 17 shows the variance of the estimated position error at 100 rpm as a function of the current load, obtained using constant V_h values and V_{hOpti}. It shows that the optimised variance of the estimated position error lies between the results for V_h

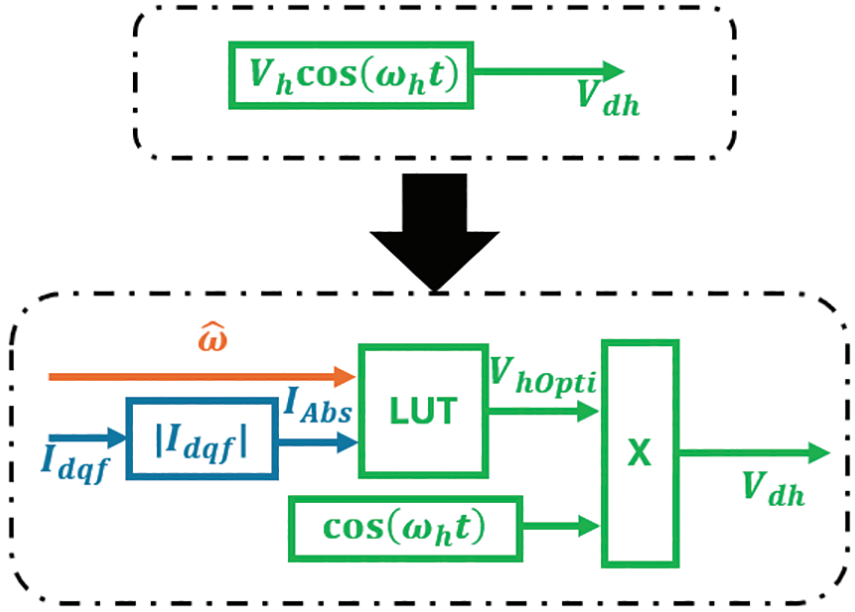

Figure 14. Experimental implementation of V_{hOpti} using LUT. LUT, look-up table.

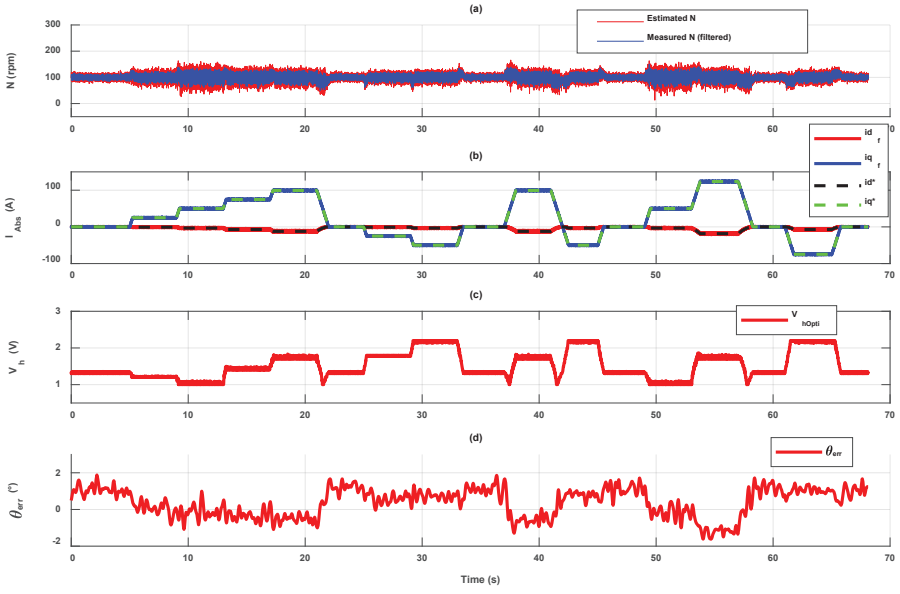

Figure 15. Experimental studied profile: (a) estimated and measured mechanical speed, (b) i_{dq} currents, (c) V_{hOpti}, (d) θ_{err} at 100 rpm.

at 1 V and 2 V. The optimisation reduces the variance of the estimated position error by 75% compared to 0.5 V and by 20% compared to 1 V, improving position quality to around 4°², equivalent to a standard deviation of 2°. Indeed, lower variance means less dispersion of the position error around its mean, improving positioning regularity and consequently system accuracy. Finally, Figure 17 confirms the $var_{\theta_{err}}$ results obtained with numerical interpolation on an experimental test cycle.

Figure 18 shows the mean position errors as a function of the current load obtained with constant V_h values and with V_{hOpti}. It can clearly be seen that the mean position error value for V_{hOpti}) lies between the $\langle\theta_{err}\rangle$ obtained for V_h equal to 1 V and 2 V, which is consistent with the V_{hOpti} values in Figure 15. The figure also shows that the

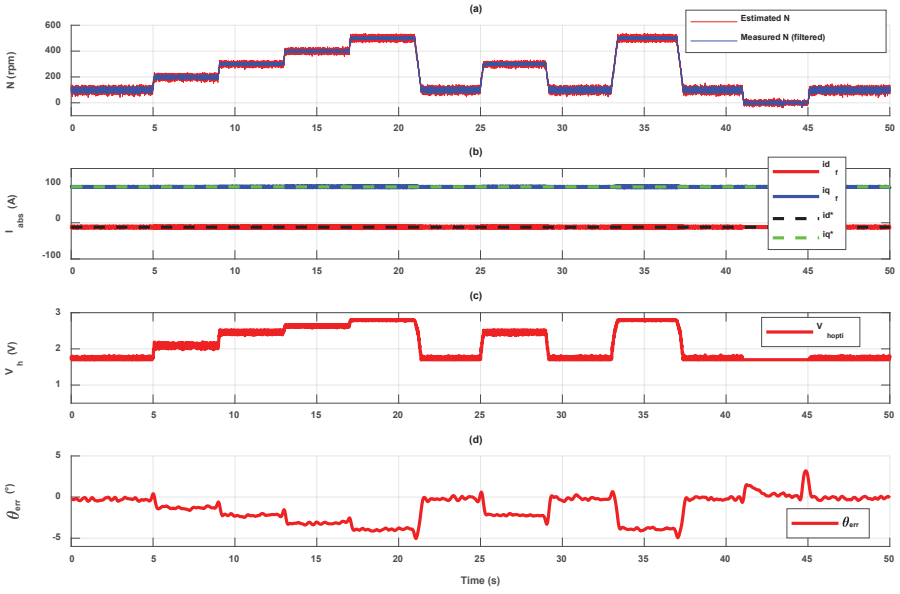

Figure 16. Experimental studied profile: (a) estimated and measured mechanical speed, (b) i_{dq} currents, (c) V_{hOpti} and (d) θ_{err} at 100 A.

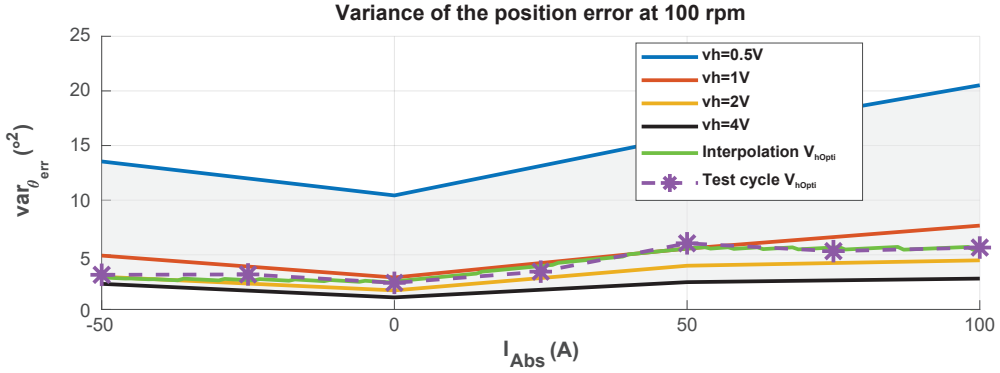

Figure 17. Impact of V_h and I_{Abs} on the variation of variance of $var_{\theta_{err}}$ at 100 rpm.

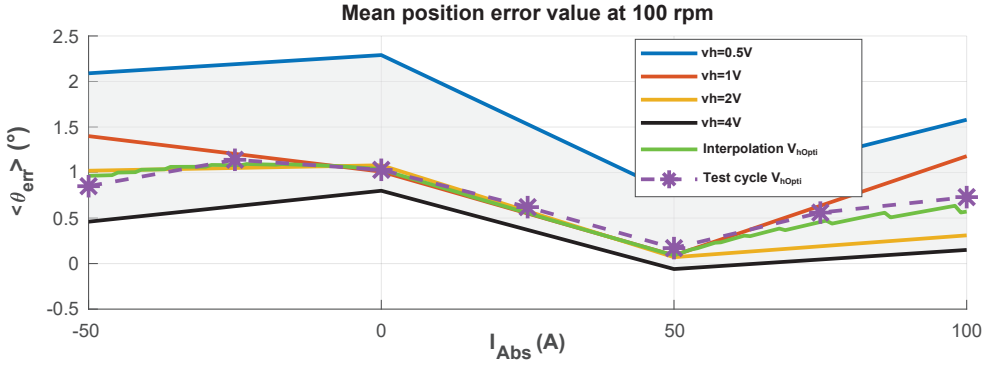

Figure 18. Impact of V_h and I_{Abs} on the variation of $\langle \theta_{err} \rangle$ at 100 rpm.

optimisation procedure reduces $\langle \theta_{err} \rangle$ by 1°compared to using V_h equal to 0.5 V. Finally, Figure 17 enables the validation of the $\langle \theta_{err} \rangle$ results obtained using numerical interpolation on an experimental test cycle.

Figure 19 illustrates the HF torque disturbance induced by the injection of HF voltage, expressed as a percentage of the average electromagnetic torque. As discussed earlier in this article, increasing V_h amplifies the disturbance to the torque, but reduces the mean position error and its variance. Figure 19 confirms the optimised ΔT_{HF} experimentally and shows that the data-driven optimisation procedure allows the optimised ΔT_{HF} to be situated between the results obtained with injections between 1 V and 2 V. Thus, it reduces ΔT_{HF} from a maximum of around 3.5% of the mean torque value with V_h equal to 4 V to 1.2% with V_{hOpti}. For 100 rpm, the comparative study shows that V_{hOpti} strikes the best balance between the three criteria: $\langle \theta_{err} \rangle$, $var_{\theta_{err}}$ and ΔT_{HF}.

The same comparison study was conducted for an example involving a constant load of 100 A and a speed variation ranging from 100 rpm to 500 rpm. Figure 20 shows the variation in the estimated position error. The optimisation reduces the variance of the error by 80% compared to 0.5 V and by 50% compared to 1 V. This improves the quality of the position and places it at around 2.5°², equivalent to a standard deviation of 1.5°.

Figure 21 shows the mean position error values as a function of mechanical speed, obtained with constant V_h values and with V_{hOpti}. Since increasing V_h decreases $\langle \theta_{err} \rangle$ and $\langle \theta_{err} \rangle$ increases with speed, V_{hOpti} is variable and increases with speed. The mean position error obtained with V_{hOpti} lies between the results for V_h equal to 2 V and 4 V, which confirms the optimised $\langle \theta_{err} \rangle$ experimentally. Figure 21 also shows that the optimisation procedure reduces the mean position error by 1° compared to the result obtained with V_h equal to 0.5 V and 1 V.

Figure 22 shows the torque disturbance caused by HF voltage injection, expressed as a percentage of the average electromagnetic torque. ΔT_{HF} depends on the current load and is independent of the speed value. The results presented in Figure 22 confirm the optimised ΔT_{HF} experimentally. As V_{hOpti} increases with the speed, the corresponding ΔT_{HF} increases from 1.4% to 2.1% falling between the results obtained with injections between 1 V and 4 V.

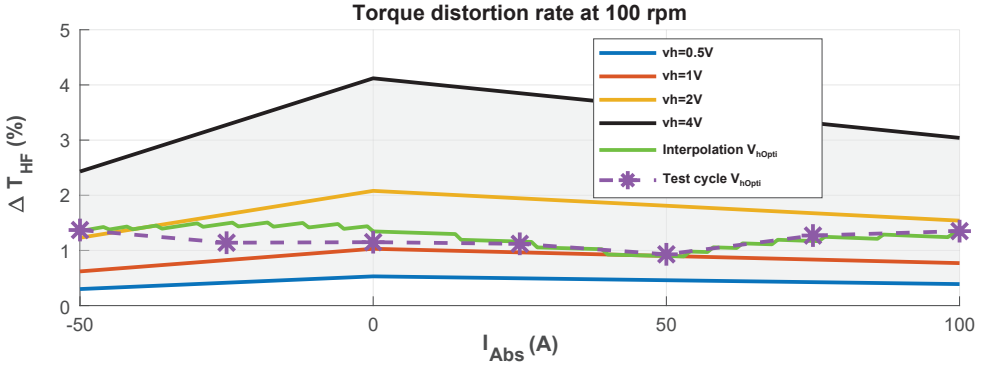

Figure 19. Impact of V_h and I_{Abs} on the variation of $\Delta T_{HF}(\%)$ at 100 rpm.

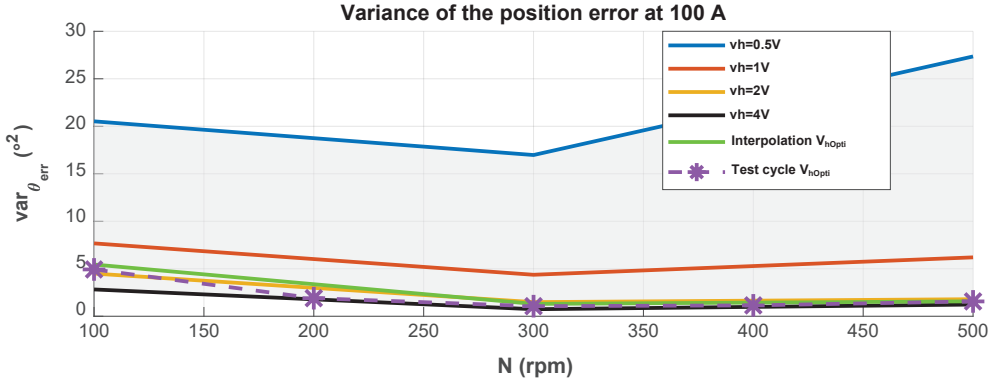

Figure 20. Impact of V_h and N on the variation of $var_{\theta_{err}}$ 100 A.

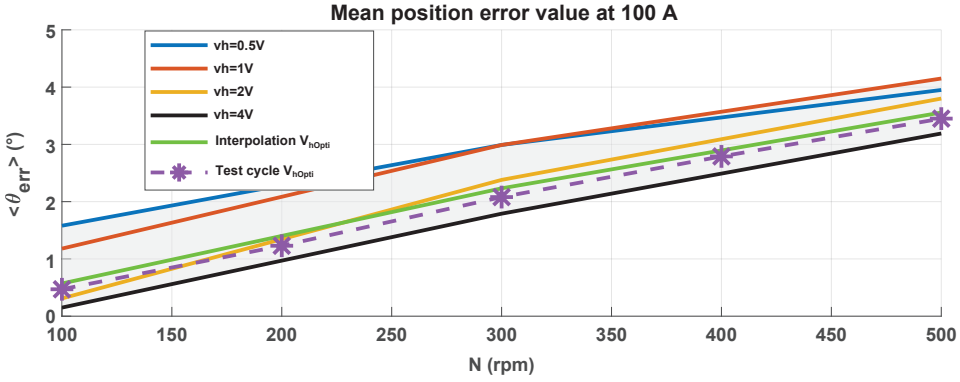

Figure 21. Impact of V_h and N on the variation $\langle \theta_{err} \rangle$ at 100 A.

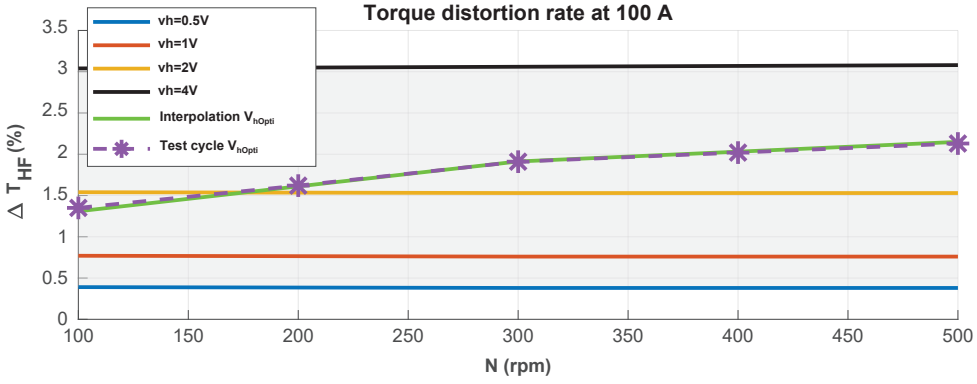

Figure 22. Impact of V_h and N on the variation of $\Delta T_{HF}(\%)$ at 100 A.

Thus, the optimisation allows to reduce ΔT_{HF} from 3% of the mean torque to 1.4% at 100 rpm. Finally, the comparison study shows that, for 100 A, V_{hOpti} strikes the best balance between the three studied criteria $\langle \theta_{err} \rangle$, $var_{\theta_{err}}$ and ΔT_{HF}.

From the previous analysis, it can be concluded that, for every operating point, using an optimally chosen voltage amplitude injection allows the best trade-off to be found in terms of position estimation quality and reduction of torque oscillations.

5. Conclusion

This paper studies an encoderless control method that uses HF voltage injection. In particular, it focuses on the pulsating carrier signal injection method. The aim is to minimise the amplitude of the injected HF voltage to reduce system disturbances, particularly torque ripples, while ensuring accurate rotor position estimation. This is of particular interest for extra-low voltage machines, such as the one studied in this article, where the effect of HF injections cannot be ignored.

The data used for the optimisation algorithm were obtained based on a reduced set of experimental tests. The proposed method relies on a reduced database consisted of 48 operating points (4 different stator current values, 3 different rotation speeds and 4 different V_h amplitudes). To enrich it, numerical interpolation was performed with a current step of 1 A, a V_h voltage step of 0.1 V and a speed step of 10 rpm.

The study shows that increasing the HF injection voltage minimises the position estimation error. However, to limit its impact on torque ripples, the voltage must be kept as small as possible. It is this balance that makes

optimisation interesting. The study also demonstrated that additional DC losses have a limited impact on the optimisation results and can be neglected.

An experimental validation was carried out to test the optimised injection strategy. This showed that implementing the optimised injection voltage, despite its magnitude constantly evolving about the operating point considered, has no impact on the motor's controllability. It also showed that a reduced experimental database is sufficient for the proposed algorithm, allowing a good compromise to be found between the quality of position estimation and torque disturbance.

References

Alfehaid, A. A., Strangas, E. G. and Khalil, H. K. (2021). Speed Control of Permanent Magnet Synchronous Motor with Uncertain Parameters and Unknown Disturbance. *IEEE Transactions on Control Systems Technology*, 29(6), pp. 2639–2646. doi: 10.1109/TCST.2020.3026569

Belghazali, H. A., Obeid, N. H., Trinh, N.-T., Id-Khajine, L. and Monmasson, E. (2024). Application of a HF signal injection sensorless method for an extra low voltage PMSynRel. In: *2024 IEEE 18th International Conference on Compatibility, Power Electronics and Power Engineering (CPE-POWERENG)*, Gdynia, Poland, 2024, pp. 1–6.

Corley, M. J. and Lorenz, R. D. (1998). Rotor Position and Velocity Estimation for a Salient-Pole Permanent Magnet Synchronous Machine at Standstill and High Speeds. *IEEE Transactions on Industry Applications*, 34(4), pp. 784–789. doi: 10.1109/28.703973

Cupertino, F., Pellegrino, G., Giangrande, P. and Salvatore, L. (2011). Sensorless Position Control of Permanent-Magnet Motors with Pulsating Current Injection and Compensation of Motor End Effects. *IEEE Transactions on Industry Applications*, 47(3), pp. 1371–1379. doi: 10.1109/TIA.2011.2126542

Holczer, A., Freijedo, F. D. and Bojoi, R. (2025). Optimal High-Frequency Injection Minimizing High-Frequency Torque Ripple for Sensorless Control of Electric Vehicle IPM Traction Motors. *IEEE Transactions on Industrial Electronics*, 72(5), pp. 4424–4435. doi: 10.1109/TIE.2024.3454189

Khan, A. A. and Mohammed, O. (2009). Wavelet filtering for position estimation of permanent magnet machine in carrier signal injection based sensorless control. In: *41st North American Power Symposium*, Starkville, MS, USA, 2009, pp. 1–5.

Kim, S.-I., Im, J.-H., Song, E.-Y. and Kim, R.-Y. (2016). A New Rotor Position Estimation Method of IPMSM Using All-Pass Filter on High-Frequency Rotating Voltage Signal Injection. *IEEE Transactions on Industrial Electronics*, 63(10), pp. 6499–6509. doi: 10.1109/TIE.2016.2592464

Lara, J., Xu, J. and Chandra, A. (2016). Effects of Rotor Position Error in the Performance of Field-Oriented-Controlled PMSM Drives for Electric Vehicle Traction Applications. *IEEE Transactions on Industrial Electronics*, 63(8), pp. 4738–4751. doi: 10.1109/TIE.2016.2549983

Li, C., Wang, G., Zhang, G., Zhao, N., Gao, Y. and Xu, D. (2021). Torque Ripples Minimization of Sensorless SynRM Drives for Low-Speed Operation Using Bi-HFSI Scheme. *IEEE Transactions on Industrial Electronics*, 68(7), pp. 5559–5570. doi: 10.1109/TIE.2020.2996133

Liu, J. M. and Zhu, Z. Q. (2014). Novel Sensorless Control Strategy With Injection of High-Frequency Pulsating Carrier Signal Into Stationary Reference Frame. *IEEE Transactions on Industry Applications*, 50(4), pp. 2574–2583. doi: 10.1109/TIA.2013.2293000

Luo, X., Tang, Q., Shen, A. and Zhang, Q. (2016). PMSM Sensorless Control by Injecting HF Pulsating Carrier Signal Into Estimated Fixed-Frequency Rotating Reference Frame. *IEEE Transactions on Industrial Electronics*, 63(4), pp. 2294–2303. doi: 10.1109/TIE.2015.2505679

Mai, Z., Xiao, F., Fu, K., Liu, J., Lian, C., Li, K., and Zhang, W. (2021). HF Pulsating Carrier Voltage Injection Method Based on Improved Position Error Signal Extraction Strategy for PMSM Position Sensorless Control. *IEEE Transactions on Power Electronics*, 36(8), pp. 9348–9360. doi: 10.1109/TPEL.2021.3055534

Makni, Z. and Zine, W. (2016). Rotor position estimator based on machine learning. In: *IECON 2016 - 42nd Annual Conference of the IEEE Industrial Electronics Society*, Florence, Italy, pp. 6687–6692.

Mizutani, R., Takeshita, T. and Matsui, N. (1998). Current Model-Based Sensorless Drives of Salient-Pole PMSM at Low Speed and Standstill. *IEEE Transactions on Industry Applications*, 34(4), pp. 841–846. doi: 10.1109/28.703990

Pasqualotto, D., Rigon, S. and Zigliotto, M. (2023). Sensorless Speed Control of Synchronous

Reluctance Motor Drives Based on Extended Kalman Filter and Neural Magnetic Model. *IEEE Transactions on Industrial Electronics*, 70(2), pp. 1321–1330. doi: 10.1109/TIE.2022.3159962

Petro, V., Kyslan, K., Bober, P. and Lacko, M. (2022). Optimization of injected voltage amplitude for low-speed sensorless control of PMSM with high-frequency pulse signal injection. In: *2022 IEEE 20th International Power Electronics and Motion Control Conference (PEMC)*, Brasov, Romania, 2022, pp. 721–727.

Raca, D., Garcia, P., Reigosa, D. D., Briz, F. and Lorenz, R. D. (2010). Carrier-Signal Selection for Sensorless Control of PM Synchronous Machines at Zero and Very Low Speeds. *IEEE Transactions on Industry Applications*, 46(1), pp. 167–178. doi: 10.1109/TIA.2009.2036551

Song, X., Fang, J., Han, B. and Zheng, S. (2016). Adaptive Compensation Method for High-Speed Surface PMSM Sensorless Drives of EMF-Based Position Estimation Error. *IEEE Transactions on Power Electronics*, 31(2), pp. 1438–1449. doi: 10.1109/TPEL.2015.2423319

Tang, Q., Shen, A., Luo, X. and Xu, J. (2018). IPMSM Sensorless Control by Injecting Bidirectional Rotating HF Carrier Signals. *IEEE Transactions on Power Electronics*, 33(12), pp. 10698–10707. doi: 10.1109/TPEL.2018.2811126

Yoon, Y.-D., Sul, S.-K., Morimoto, S. and Ide, K. (2011). High-Bandwidth Sensorless Algorithm for AC Machines Based on Square-Wave-Type Voltage Injection. *IEEE Transactions on Industry Applications*, 47(3), pp. 1361–1370. doi: 10.1109/TIA.2011.2126552

Yousefi-Talouki, A., Pescetto, P., Pellegrino, G. and Boldea, I. (2018). Combined Active Flux and High-Frequency Injection Methods for Sensorless Direct-Flux Vector Control of Synchronous Reluctance Machines. *IEEE Transactions on Power Electronics*, 33(3), pp. 2447–2457. doi: 10.1109/TPEL.2017.2697209

Zhao, W., Jiao, S., Chen, Q., Xu, D. and Ji, J. (2018). Sensorless Control of a Linear Permanent-Magnet Motor Based on an Improved Disturbance Observer. *IEEE Transactions on Industrial Electronics*, 65(12), pp. 9291–9300. doi: 10.1109/TIE.2018.2823660

Zine, W., Makni, Z., Monmasson, E., Idkhajine, L. and Condamin, B. (2018a). Interests and Limits of Machine Learning-Based Neural Networks for Rotor Position Estimation in EV Traction Drives. *IEEE Transactions on Industrial Informatics*, 14(5), pp. 1942–1951. doi: 10.1109/TII.2017.2765398

Zine, W., Idkhajine, L., Monmasson, E., Makni, Z., Chauvenet, P., Condamin, B. and Bruyere, A. (2018b). Optimisation of HF Signal Injection Parameters for EV Applications based on Sensorless IPMSM Drives. *IET Electric Power Applications*, 12, pp. 347–356. doi: 10.1049/iet-epa.2017.0228